JOURNAL OF Applied Polymer SCIENCE

# Probing the Reinforcing Mechanism of Graphene and Graphene Oxide in Natural Rubber

**Fayong Li, Ning Yan, Yanhu Zhan, Guoxia Fei, Hesheng Xia**
State Key Laboratory of Polymer Materials Engineering, Polymer Research Institute, Sichuan University, Chengdu 610065, People's Republic of China
Correspondence to: G. Fei (E-mail: 403450356@qq.com)

**ABSTRACT:** Natural rubber (NR) containing graphene (GE) and graphene oxide (GO) were prepared by latex mixing. The *in situ* chemically reduction process in the latex was used to realize the conversion of GO to GE. A noticeable enhancement in tensile strength was achieved for both GO and GE filled NR systems, but GE has a better reinforcing effect than GO. The strain-induced crystallization was evaluated by synchrotron wide-angle X-ray diffraction. Increased crystallinity and special strain amplification effects were observed with the addition of GE. The incorporation of GE produces a faster strain-induced crystallization rate and a higher crystallinity compared to GO. The entanglement-bound tube model was used to characterize the chain network structure of composites. It was found that the contribution of entanglement to the conformational constraint increases and the network molecular parameters changes with the addition of GE and GO, while GE has a more evident effect than GO. © 2013 Wiley Periodicals, Inc. J. Appl. Polym. Sci. 129: 2342–2351, 2013

**KEYWORDS:** composites; nanotubes; graphene and fullerenes; mechanical properties

Received 30 October 2012; accepted 23 December 2012; published online 17 January 2013
**DOI: 10.1002/app.38958**

## INTRODUCTION

Natural rubber (NR) is an indispensable material in industrial applications such as pneumatic tires and vibration isolation systems due to its excellent elastic property, and good cracking resistance. Strain-induced crystallization (SIC) in vulcanized NR is well recognized as the main factor responsible for improvements in the mechanical properties of NR.[1–4] The influence of fillers on SIC of rubber has been extensively studied by synchrotron wide-angle X-ray diffraction (WAXD), birefringence, and infrared dichroism.[5–11] The preferred chain orientations and remarkable enhancement of SIC were observed in filled NR. The crystallinity is found to vary with the filler content. Graphene (GE) is a novel filler with a thin-layered 2D structure and excellent mechanical properties, such as high modulus and tensile strength.[12,13] GE has been used to prepare NR composites by an ultrasonically assisted latex mixing and *in-situ* reduction process.[14,15] The mechanical properties are significantly improved even with a low addition of GE ($\leq$2%), which is not achieved for other conventional fillers.[16–18] However, the knowledge on the influences of GE on the rubber network parameters is lacked although it is crucial in gaining insight into the reinforcing mechanism of NR/GE nanocomposites.

The molecular statistical basis of unfilled crosslinked and entangled polymers was established by Ronca and Allegra,[19] Kastner,[20] and Flory.[21] These theories assume that the restricted phase space (due to entanglements) available to the chains only affects crosslink fluctuations. Some studies[22–25] revealed that the configurational constraint of the entire network chain is important in explaining the stress–strain behavior of the crosslinked network. Edward[26,27] developed the concept by assuming that the entanglement act along the entire contour length of the network chain segments via constraining virtual tubes around the network chains. The tube model is shown to allow proper crosslink separation and constraint contribution to the stress–strain behavior. It is a reliable theoretical basis for stress–strain treatment to determine the network parameters of the unfilled rubber. However, the situation drastically differs in the case of the filled rubber network. The filled composites are regarded as a "rubbery" continuous phase, a particulate "rigid" phase, and a transition zone between the highly immobilized bound rubber (BdR) phase and mobile bulk rubber phases.[28] Funt et al.[29] first proposed an entanglement bound rubber tube (EBT) model to describe the contribution of entanglement, which has been subsequently used to describe the effects of CB[30] and clay[31] on the mechanical behavior of rubber. However, few work is concerned on the influence of GE and graphene oxide (GO) on the NR network structure through the EBT model.

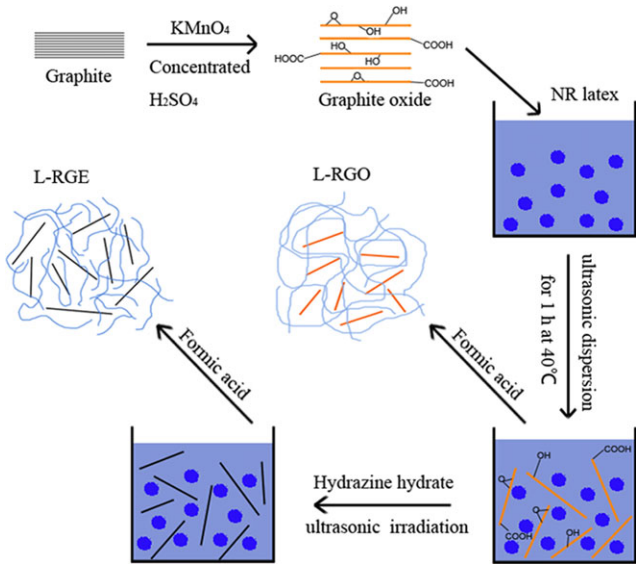


**Figure 1.** Schematic illustration of the preparation of NR/GE and NR/GO composites. [Color figure can be viewed in the online issue, which is available at wileyonlinelibrary.com.]

The main objective of this work is to reveal the reinforcing mechanism of GE-filled NR composites through SIC and EBT model. The influences of GE and GO on the crystallinity during stretching were monitored by the synchrotron WAXD. The contribution of entanglement to the mechanical property was estimated in terms of the EBT model. The network parameters of the unfilled and filled NR were calculated by applying the proposed EBT to the stress–strain experiment. The results provide new insights into the discrepancy of the reinforcing effect between GE and GO in NR.

## EXPERIMENTAL

### Material

The commercial used NR in this study was NR (SCR 5) from Yunnan Natural Rubber Industry Company, Kunming, China. NR latex (NR content: 60 wt %) was purchased from Chengdu Fangzheng Company (China). Flake Graphite with an average thickness of ~75 $\mu$m was obtained from Qingdao Dahe Graphite Company (China). Potassium permanganate ($KMnO_4$) was obtained from Chongqing Boyi Chemical Reagent Company (China). Concentrated sulfuric acid ($H_2SO_4$) and hydrochloric acid (HCl) were all of analytical-grade and obtained from Sichuan Xilong Chemical Company (China). Hydrazine hydrate was purchased from Chendu Kelong Chemical Reagent Company (China). Hydrogen peroxide (30%) was provided by Tianjin Zhiyuan Chemical Reagent Company (China). Formic acid was purchased from Tianjin Bodi Chemical Reagent Company (China). Other reagents including vulcanization agent sulfur, zinc oxide (ZnO), accelerator *N*-cyclohexyl-2-benzothiazole-sulfenamide (CBS), 2-mercaptobenzothiazole (MBT), and 4-Isopropylaminodiphenylamine (4010NA), and stearic acid (SA) are all commercially available.

### Preparation of the NR Composites

NR/GE and NR/GO composites were prepared through the previous route called ultrasonically assisted latex mixing and *in-situ* reduction process.[14] The procedure was schematically represented in Figure 1. First, natural flake graphite was oxidized to GO according to the Hummer's method.[32] Then, 2.5 mg/ml GO aqueous solution was prepared by bath sonication (KQ-250DE, 40 KHz, Kunshan Ultrasonic Instrument Company, China) at 40°C for 1 h. Then an appropriate quantity (16.6 g) of NR latex was sequentially dispersed into the GO solution by sonication for 1 h. After the coagulation and drying process, NR/GO master batches were obtained. For the preparation of the NR/GE master batch, hydrazine hydrate was added into the GO/NRL and then the mixture was subjected for sonication. After the coagulation and drying process, the NR/GE masterbatch was obtained. Vulcanized NR samples were prepared in an open twin roll mill at room temperature according to the recipes outlined in Table I. The resultants were compression molded into sheets at a curing temperature of 150°C and a pressure of 10 MPa for the optimum curing time determined on the basis of result of the cure characteristics from Rheometer R100E instrument (Youshen, China), and then cooled for 3 min under pressure at room temperature.

### Characterization

Synchrotron WAXD experiments were carried out at room temperature using a U7B beamline in the National Synchrotron Radiation Laboratory, Hefei, China. The wavelength was 0.154 nm. The specimen was simultaneously stretched horizontally to the predetermined elongation at a strain rate of 10 mm/min in a symmetric fashion, allowing the X-ray to irradiate almost the same specimen position. The exposure time for each image was 180 s. The 2D WAXD patterns were recorded using a Mar CCD 165 X-ray detector system. The Fit2D software package was used to analyze the 2D WAXD patterns.

The tensile strength was tested using an Instron (5567) universal test machine at room temperature and at a rate of 500 mm/min according to the GB/T528-1998 standard. The sample initial width and thickness were 4 and 2 mm, respectively. Five parallel measurements of each sample were carried out and the average value was presented.

The network chain density ($\nu_e$) was determined by a rapid solvent swelling method. The samples were cut into rectangular

**Table I.** Recipes of NR Composites

| Samples (phr)[a] | NR | GO/NR | GE/NR |
|---|---|---|---|
| Filler content (wt %) | 0 | 0.3/0.7/1.0 | 0.3/0.7/1.0 |
| Raw NR | 90 | 90 | 90 |
| NR/Filler masterbatch | 0 | 10 | 10 |
| Zinc oxide | 5 | 5 | 5 |
| Stearic acid | 2 | 2 | 2 |
| Sulfur | 3 | 3 | 3 |
| Antioxidant (4010NA) | 2 | 2 | 2 |
| Accelerator (CBS [b]) | 1.5 | 1.5 | 1.5 |
| Accelerator (MBT [c]) | 0.1 | 0.1 | 0.1 |

[a]Parts per hundred parts of rubber.
[b]*N*-cyclohexyl-2-benzothiazole-sulfenamide.
[c]2-mercaptobenzothiazole.

Applied Polymer SCIENCE

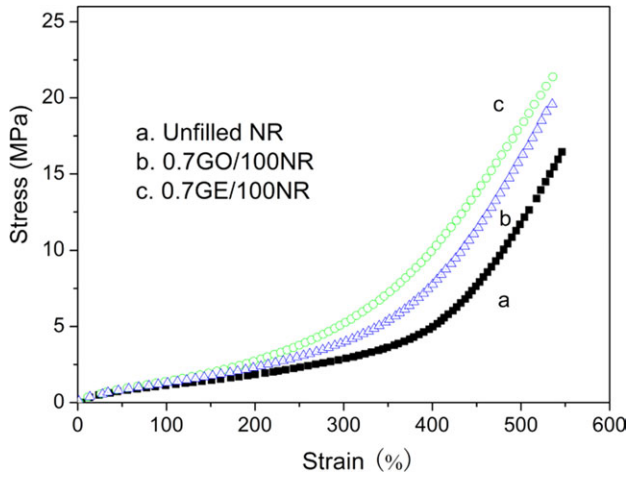


**Figure 2.** Stress–strain curves for the unfilled NR and filled NR composites. [Color figure can be viewed in the online issue, which is available at wileyonlinelibrary.com.]

pieces (10 mm × 10 mm × 2 mm) and weighed before and after soaking in toluene for 7 days to ensure equilibrium conditions. The crosslink density was calculated using the Flory–Rehner eq. (1).[33]

$$\nu_e = \rho/M_c = -[\ln(1-\nu_r) + \nu_r + \chi_1 \nu_r^2]/[\nu_1(\nu_r^{1/3} - \nu_r/2)] \quad (1)$$

where, $\nu_e$ is the network chain density (mol/cm$^3$), $\rho$ is the rubber density (0.92 g/cm), $M_c$ is the average molecular weight between the network crosslinks, $\nu_r$ is the volume fraction in a swollen network ($\nu_r = \nu_{rubber}/\nu_{rubber}+\nu_{toluene}$), $\nu_1$ is the molar volume of toluene (106.2 ml/mol), and $\chi_1$ is the Flory–Huggins interaction parameter (0.393 for the NR/toluene) between toluene and rubber.

The filler–rubber interaction in the composite was evaluated by the Lorenz and park eq. (2).[34]

$$Q_f/Q_g = ae^{-z} + b \quad (2)$$

where, $f$ and $g$ refer to filled and neat rubber, respectively, $z$ is the ratio of filler weight to the rubber hydrocarbon in the vulcanizates, and $a$ and $b$ are constants. The cured sample is cut into dimensions of 30 mm × 5 mm × 2 mm, and then immersed in toluene until equilibrium swelling for 48 h at 25°C. The samples were dried in an oven at 60°C until constant weights were obtained. The toluene uptake per gram of rubber ($Q$) was determined using eq. (3).

$$Q = (w_s - w_d)/(w_o \times \varphi_{rubber}) \quad (3)$$

Higher $Q_f/Q_g$ values denote lower interaction extents between the filler and matrix. $w_s$ is the swollen weight, $w_d$ is the dried weight, $w_o$ is the original weight, and $\varphi_{rubber}$ is the mass fraction of the rubber in the composites.

The bound rubber content was tested based on the method reported by Leblanc et al.[35] An amount of 0.5 g of uncured sample was cut into small pieces and introduced in a previously weighed steel wire net ($m_1$). The net was closed and weighed ($m_2$), and then immersed in toluene for 72 h at room temperature during which the sample was washed with fresh solvent every 24 h. The net was slowly removed from the solvent and dried for a few hours at 40°C in a vacuum oven until a constant weight ($m_3$) was achieved. The amount of bound rubber (as the weight percent, wt %) of the initial rubber content of the uncured sample was given by eq. (4).

$$BdR(\%) = \frac{m_0 - (m_2 - m_3)}{m_0} \times 100 \quad (4)$$

where, $m_0$ is the rubber content in the sample given by $m_0 = (m_2 - m_1)\times 100/\varphi_{rubber}$ ($m_1$ is the mass of the empty net and $\varphi_{rubber}$ is the mass fraction of the rubber in the composites.), $m_2$ is the mass of the net plus the unextracted sample, and $m_3$ is the mass of the basket plus the extracted dried sample.

## RESULTS AND DISCUSSION

### Stress–Strain Behavior

The typical stress–strain curves of the unfilled NR and NR composites containing GE or GO are shown in Figure 2. The tensile strengths are listed in Table II. The NR shows a significant improvement in tensile strength due to the inclusion of a small amount of GE and GO. The tensile strength increased from 16.5 MPa for unfilled NR to 25.4 MPa for the NR/GE composite containing 1 phr GE. The GO/NR composites containing 1 phr GO has a tensile strength of 21.2 Mpa, lower than that of GE/NR composites. Clearly, GE has a better reinforcing effect on NR than GO. If using conventional filler such as carbon black, a much higher loading must be adopted to achieve the same improvement effect of GE,[14,15] which suggests a higher GE reinforcing efficiency. A further investigation in these reinforcing effects was conducted experimentally by Synchrotron WAXD and theoretically through the Entanglement-Bound Rubber Tube Model.

### SIC

SIC is recognized as the main reason for the improvement in the tensile properties of NR. Crystallites can play a role as a filler analog and additional crosslinking point in the network, which contributes to the enhancement in the tensile strength. The discrepancy in the different reinforcing effect of GE and GO on the SIC deserves to be investigated in detail.

The typical evolutions of the WAXD patterns of the selected NR composites and unfilled NR during stretching are shown in Figure 3. All images were normalized with respect to the sample

**Table II.** Tensile Strength of Unfilled NR and Filled NR Composites

| | Tensile strength (MPa) | |
|---|---|---|
| Filler content (phr) | GO/NR | GE/NR |
| 0 | 16.5 ± 0.3 | 16.5 ± 0.3 |
| 0.3 | 17.2 ± 0.9 | 20.5 ± 0.3 |
| 0.7 | 19.8 ± 1.3 | 22.1 ± 0.8 |
| 1 | 21.2 ± 1.0 | 25.4 ± 1.5 |

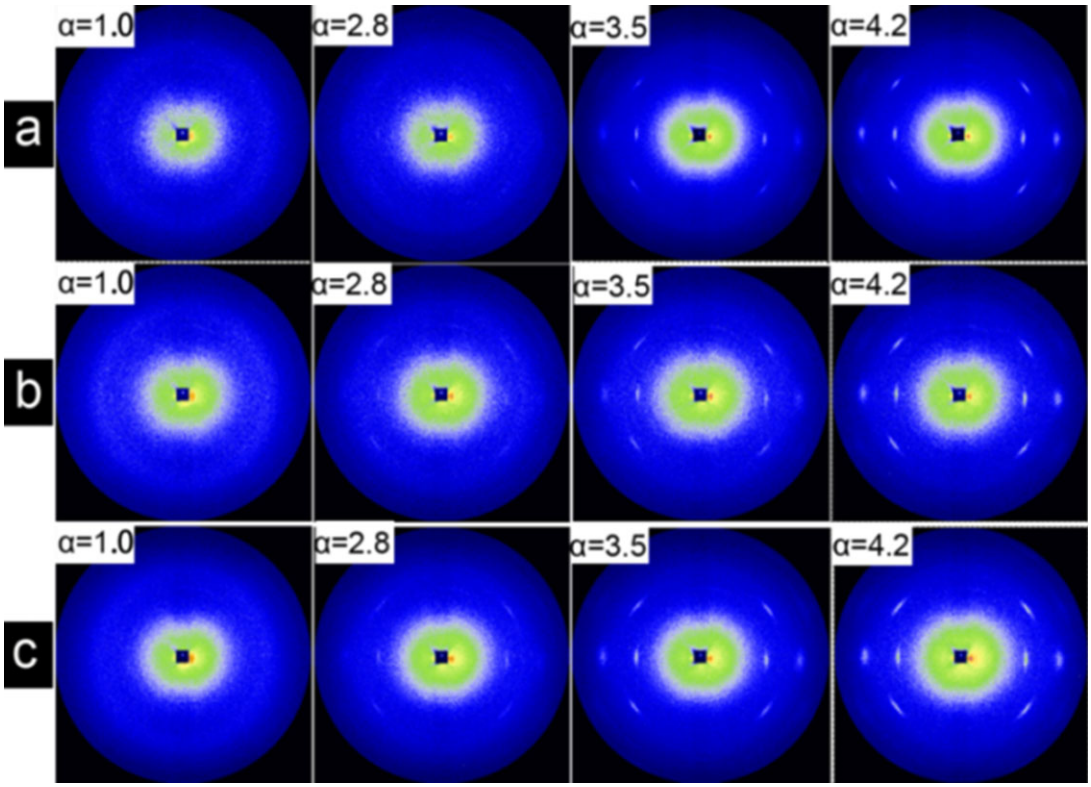


**Figure 3.** Sequential changes of WAXD patterns from (a) NR (b) 0.7GO/NR and (c) 0.7 GE/NR. Corresponding strain (α) values are indicated at the left top in each pattern. [Color figure can be viewed in the online issue, which is available at wileyonlinelibrary.com.]

thickness change, sample absorption, and beam fluctuation. The intensities of these reflections increase with strain during stretching. For the GE/NR composites, the oriented crystalline reflection peaks start to appear at a smaller strain than that for GO/NR composites. Also the diffraction intensity is stronger compared with unfilled NR and GO/NR at the same strain. After subtracting the air scattering from the starting WAXD patterns using Fit2D software, the corrected WAXD patterns were integrated along the azimuthal direction from 0° to 360°. The resultant diffraction profiles taken along the equatorial of the 2D WAXD patterns were decomposed by 1D fitting[38] into several peaks. Each peak was fitted with the Gaussian function represented in eq. (5).

$$I(x)=h\exp\left[-(x-x_c)^2/2w^2\right] \tag{5}$$

Where, $I(x)$ is the intensity at position $x$, $x_c$ is the position at the scattering maximum, and $h$ and $w$ are the parameters related to the peak height and peak width, respectively. The equatorial reflection peak intensities of $I_{eq}(200)$ and $I_{eq}(120)$ were used to evaluate the crystallinity. The mass fraction of the strain-induced crystal can be estimated by dividing the sum of the crystal diffraction intensity by the total scattered intensity. The crystallinity calculation from the resultant Gaussian peak is described as eq. (6).

$$X_c = \frac{A_c}{A_c + A_a} \tag{6}$$

where, $A_c$ and $A_a$ represent the integrated intensities of the crystalline and amorphous regions, respectively.

Figure 4 shows the variation of crystallinity with strain for unfilled NR, 0.7GO/NR and 0.7GE/NR. The crystallinity of the filled sample is higher than that of unfilled NR at the same strain and the NR/GE composite has the highest crystallinity among the three kinds of materials. NR self-reinforcement has long been recognized

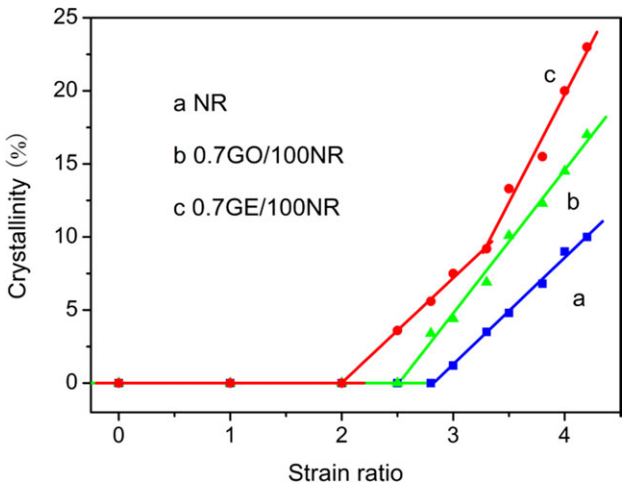


**Figure 4.** Crystallinity as a function of strains for unfilled NR and NR composites. [Color figure can be viewed in the online issue, which is available at wileyonlinelibrary.com.]

Applied Polymer SCIENCE

**Table III.** Onset Strain Ratios of Crystallization for Unfilled NR and Filled NR

| Samples | BdR (%) | Onset strain ratio of the crystallization | | |
|---|---|---|---|---|
| | | $\alpha^{O}$ [a] | $\alpha_r^{O}(\varphi)$[b] | $\alpha_r^{O}(b)$[c] |
| NR | 0 | 2.8 | 2.8 | 2.8 |
| GO (0.7 phr) /NR | 7.4 | 2.5 | 2.5 | 2.6 |
| GE (0.7 phr) /NR | 13.1 | 2.0 | 2.0 | 2.2 |

[a]The experimental values.
[b]The corrected values considering the filler volume fraction.
[c]The corrected values considering the volume fraction of the fillers plus bound rubber.

to originate from the SIC. The strain-induced crystallites act as additional crosslink points and, to some extent, as the fillers that increase the efficiency of the crosslink in the network, which is an important factor in tensile strength enhancement for NR.

The onset strain of crystallization ($\alpha^0$) was determined by the interception of the linear regression lines in the plot of crystallinity against strain.[9,11] The calculated $\alpha^0$ value of the selected unfilled NR, 0.7GO/NR and 0.7GE/NR samples were 2.8, 2.5, and 2.0, respectively. It is clear that the $\alpha^0$ shifts to a lower value for the filled NR samples. This trend is more noticeable in the samples filled with GE than that with GO. This larger strain amplification due to the effective strain of the rubber portion than the nominal macroscopic one in the filled NR was reported by assuming filler un-deformable.[5,8–11] The relationship between the effective strain ratio and volume fraction ($\varphi$) of the filler is formulated as eq. (7).[10]

$$\alpha_r(\varphi) = (\alpha - \varphi)/(1 - \varphi) \tag{7}$$

The $\alpha^0$ values are converted in terms of eq. (7), as listed in Table III. The corrected value $\alpha_r^0(\varphi)$ does not change compared with the experimental values ($\alpha^0$), and this was attributed to the low filler content. In filled rubber, the bound rubber layer formed around the filler particle through the intense physical and chemical interactions also can be considered immobile,[29] and it is assumed to be the un-deformable component like filler. The discrepancy of the strain amplification effect for the 0.7GE/NR and 0.7GO/NR samples can be interpreted by considering the contents of bound rubber in the two composites. The measured bound rubber contents using Leblanc and Hardy's methods[35] are 7.4% and 13.1% for the 0.7GO/NR and 0.7GE/NR samples, respectively. The corrected values of the onset strain $\alpha_r^0(b)$ considering the filler plus bound rubber volume fraction are shown in Table III. The corrected $\alpha_r^0(b)$ values for filled NR are closer the uncorrected values $\alpha^0$, but still much smaller than the onset strain of unfilled NR. It is different from the carbon black-filled NR whose corrected onset strain of crystallization for the filler volume fraction is similar to the unfilled NR.[10] A similar phenomenon was reported in the nano-alumina filled NR composites,[9] where an alternative mechanism of filler effect was thought to dominate the rubber network structure and strain amplification effect. On the other hand, the GE or GO particles can act as nucleation centers of the NR crystallites. According to the work reported by Rault et al.,[39] after the addition of filler, the extension of the chains in this heterogeneous rubber became nonuniform, the chains were overstrained and the crystallization was accelerated around particles. The unfilled NR and 0.7GO/NR exhibit a single crystallization step, whereas 0.7GE/NR has two, as shown in Figure 4. The slope values ($S$) of the regression line of unfilled NR and 0.7GO/NR composite are 0.07 and 0.1, respectively. The 0.7GE/NR composite shows a similar slope value of 0.07 as that of unfilled NR within a strain range of 2.0–3.3, whereas a larger slope value of 0.15 is observed when the strain is greater than 3.3. This result reveals that GE accelerates the SIC rate at a large deformation. Weng et al.[11] thought that the sub-network orientation at relatively low strains precedes the onset strain of crystallization in filled NR, inducing the filler orientation at an early stage. Further development of the filler orientation can also enhance the sub-network orientation, which is the SIC origin. The lower $\alpha^0$ for 0.7GE/NR reveals an occurrence of earlier orientation of subnetwork chains, which results from the high interaction level between polymer chains and GE due to the high specific area of GE.

### Lateral Crystallite Size

The widths of the 200 and 120 reflections were estimated. The intensity distribution from the eq. (5) was used to evaluate the crystallite size. Each peak width ($w$) value was converted into the half-width $\beta_{hkl}$ (represented by radian) according to the procedure described by Tosaka.[40] The crystallite size was estimated using the Scherrer eq. (8).

$$L_{hkl} = k\lambda/(\beta_{hkl}\cos\theta) \tag{8}$$

where, $L_{hkl}$ is the crystallite size in the direction perpendicular to the ($hkl$) plane, $\lambda$ is the wavelength, and $\theta$ is the Bragg angle. Scherrer factor $k$ is 0.89 when $\beta_{hkl}$ is the half width of the ($hkl$) reflection in the radial direction.[41] Figure 5 shows the variations in the $L_{200}$ and $L_{120}$ crystallite sizes during the stretching process. Both $L_{200}$ and $L_{120}$ show a similar trend, i.e., decreased crystallite size with the strain for the selected samples. The reason is as follows: the mean distance between the stretched chains acting as nuclei during SIC decreases, accordingly, the average crystallite size becomes smaller.[41] The unfilled NR shows larger crystallite sizes compared to the filled GO/NR and GE/NR samples in the same strain. The GE/NR has a smaller crystallite size than GO/NR. These results suggest that both GO and GE fillers can act as the nuclei to induce the formation of crystallite during stretching. GE has a better nucleation function possibly due to the stronger interaction between GE and rubber.

### EBT Model for GE–Rubber Composites

To gain insight into the reinforcing effect of GE on NR on the molecular level, the EBT model[29] was used to analyze the microstructure of the rubber network. The EBT model allows a proper separation of crosslinks and constraint contribution to the stress–strain behavior and a reliable determination of crosslink densities. The topological constraint was assumed to act on the entire network chains to restrict them from fluctuating within small length scale by packing effects that result from the inability of the chains to pass through their neighbors.

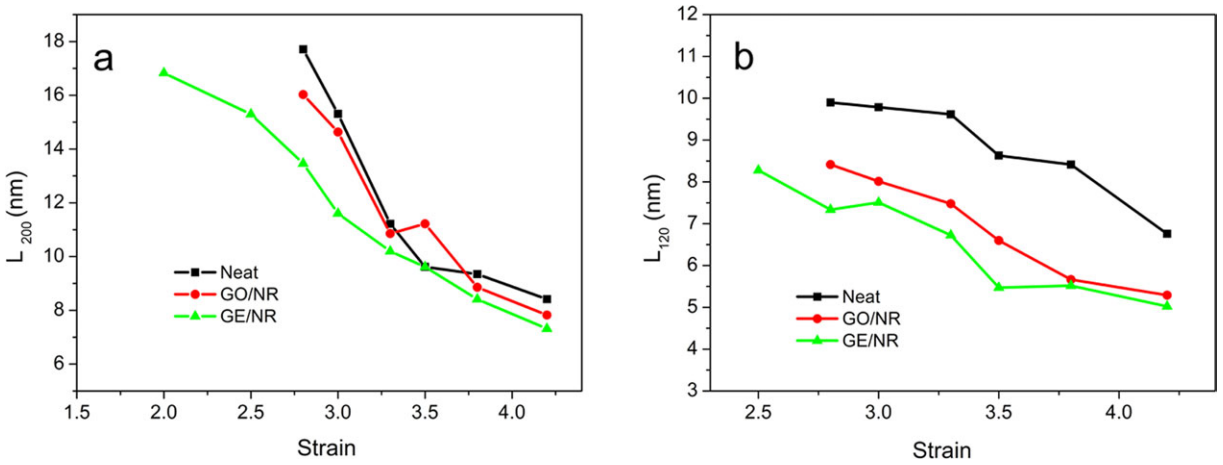


**Figure 5.** Variations in the lateral crystallite sizes: (a) $L_{200}$ and (b) $L_{120}$ during stretching. [Color figure can be viewed in the online issue, which is available at wileyonlinelibrary.com.]

Configurational tubes were introduced successfully which have their origin in studies of the dynamics of long polymer molecules in melts. In rubbers the tube becomes frozen due to quenching by crosslinks, which preserves the local topology, and fluctuations on large length scales are hindered by chemical crosslinks.

According to the EBT model, the elastic free energy $w_f$ that considers the finite extensibility of the chain together with the tube constraint can be expressed by two elastic moduli $G_c$ and $G_e$, which are closely related to the Mooney–Rivlin eq. with constants C1 and C2.[42] The nominal stress $\sigma$ is obtained by the differentiation $\sigma = \partial w_f / \partial \alpha$.[43] The stress–strain relation in Figure 2 can be expressed as eqs. (9) and (10).

$$\sigma* = \frac{\sigma}{\alpha - \alpha^{-2}} = G_c + G_e f(\alpha) \tag{9}$$

$$f(\alpha) = \frac{2}{\beta}\frac{\alpha^{\beta/2} - \alpha^{-\beta}}{\alpha^2 - \alpha^{-1}}, f(\alpha = 1) = 1 \tag{10}$$

where, $\alpha$ is the strain and $f(\alpha)$ is strain function. $G_c$ is the elastic modulus corresponding to the crosslink constraint, and $G_e$ is entanglement modulus corresponding to the topological tube-like constraint. $\beta$ can be considered as an empirical parameter which describes the relaxation of the deformed tube in the deformed state to an undeformed tube corresponding to the equilibrium state, $\beta \sim 1$.[30] In the case of filled rubbers, $\alpha$ (appropriate in the rubber matrix) should be replaced by the intrinsic tension ratio $\alpha'$ eqs. (11) and (12).

$$\alpha' = (\alpha - 1)\chi_{eff} + 1 \tag{11}$$

$$\chi_{eff} = 1 + 2.5\varphi_{eff} + 14.1\varphi_{eff}^2 \tag{12}$$

where, $\varphi_{eff}$ is the effective filler volume fraction, and $\chi_{eff}$ is the effective amplification factor. However, in our case, the effective volume fraction of the fillers $\varphi_{eff}$ is quite low (0.57%). Thus, $\alpha$ is approximated to $\alpha'$.

$G_e$ is associated with the lateral dimensions of the configurational tubes within the bulk rubber by the eq. (13).

$$G_e = \frac{v_s l_s^2 k_B T}{4\sqrt{6} d_0^2} \tag{13}$$

where, $v_s$ is the density of the statistical segments taken as 3.85/nm,[31] $k_B$ is the Boltzmann constant, and $T$ is the temperature. $l_s$ is the average length of Kuhn's statistical segment (0.88 nm for NR). The lateral tube dimension ($d_0$) correlates to the mean number of statistical segments between two successive entanglements ($n_e$) is expressed as eq. (14):

$$d_0 = l_s\sqrt{n_e} \tag{14}$$

The root-mean-square end-to-end distance of the mobile network chains $R_c$ related to the average molecular mass of these chains is estimated as eq. (15), where $M_c$ is the average molecular weight between the network crosslinks. $M_s$ is the molar mass of the statistical segments (for NR, the $M_s$ = 67.7 g/mol)

$$R_c = l_s(M_c/M_s)^{0.5} \tag{15}$$

According to eqs. (9) and (10), the stress–strain curves in Figure 2 are represented in the form of a Mooney–Rivlin plot, $\sigma^*$ vs. ($\alpha$) in Figure 6, where $\sigma^*$ is the reduced stress and ($\alpha$) is shown in the eq. (1). $l_0$ is the initial length of the sample and $l$ is the elongated one. The stress initially decreases a little bit with the increased strain $\alpha$ due to the slippage of the entanglement.[30] This effect is more evident in the case of the filled composites, which is reflected in the higher slope of intermediate deformation in the Mooney plot, as shown in Table IV. However, the stress rapidly increases again at higher strains. A noticeable upturn can be observed at the high strain region, which was attributed to SIC[36] and the finite extensibility of the chains.[37] From Figure 6, it is noted that the GE/NR composite shows an upturn at a smaller strain than the GO/NR composites, indicating that GE is more helpful for the SIC.

Based on the molecular statistical approach, the EBT theory is not fulfilled at large strains. Thus, our analysis is based on the intermediate deformation in the Mooney plot.[42] The parameters

Applied Polymer SCIENCE

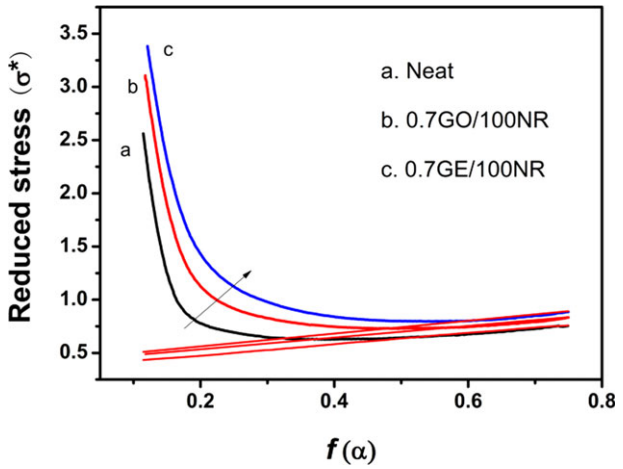


**Figure 6.** Mooney–Rivlin plots of the unfilled NR and filled NR, the red line is the fitting linear of the linear part in the intermediate deformation. [Color figure can be viewed in the online issue, which is available at wileyonlinelibrary.com.]

$G_e$ and $G_c$ can be determined from the slope and y-axis interception of the linear part of the intermediate deformation, respectively, as shown in the Mooney plot $\sigma^*$ vs. ($\alpha$) (Figure 6) according to eqs. (9) and (10).[30] The network parameters of the samples are summarized in Table IV. Both network parameters $G_c$ (contributed by the chemical crosslink) and $G_e$ (related to the topological tube like constraint) has a increase trend with the addition of filler and $G_e$ increases more. The average molecular mass of the network chains is related to $G_c$ according to the relation $M_c = \rho_p RT/G_c$, where $\rho_p$ is polymer density. The decrease of $M_c$ with increasing GE content is equivalent to an increase in the formation of polymer–filler couples and short bridging chains between filler particles which enlarge the extension of the filled network or of highly bounded clusters of filler particles.[31] Comparing to the 0.7GO/NR systems, the increasing in the $G_c$ and $G_e$ for 0.7GE/NR is more evident. This result is attributed to the stronger interfacial interactions between GE and rubber. The EBT model is schematically represented in Figure 7 to visualize the effect of the filler on the rubber chain network structure.

According to the EBT model it is assumed that a number of entanglements are formed in the transition zones between the tightly adsorbed bound and bulk rubbers far from the filler surface phases, which are believed to dominate the rubber property.[30] The transition zones contribute to the increase in the $G_c$ and $G_e$ because of the strong filler–rubber interaction. The molecular network parameters can be calculated according to the eqs. (13)–(15) and the data are summarized in Table IV. With the addition of the filler the tube dimension $d_0$ decreases, also the mean number of Kuhn's statistic chain segments between two successive entanglements ($n_e$), and the average molecular mass of the chain ($M_c$) decrease. Our results are similar with those for rubber network filled with clay reported by López-Manchado et al.[31] but different with the carbon black filled rubber.[30] This is because carbon black normally forms large agglomerates in elastomer, while the well dispersed GE or GO nanoplatlets with high specific surface area and nanoscale surface roughness have more chance to interact with rubber. The GE or GO nanoplatlets are characterized by a high aspect ratio, so the optimum dispersion of even a small quantity of nanolayer is enough to interact with rubber matrix and will make only a few rubber chains remain free. TEM micrographs confirm the homogeneous dispersion of GE in NR matrix in our previous report.[14] So, as corroborated from molecular network parameters, the addition of GE or GO reduces the tube dimensions, by the presence of neighboring chains, which restricts the movement of the rubber chains to a lower volume. The polymer is nanoscopically confined, forming a highly ordered and entangled structure due to the intense filler-interactions, which limit the lateral fluctuation of the chain to a lower volume and reduce the number of possible chain configuration associated to the chain entropy.[31] Also, a larger decrease of the tube dimension is observed for the sample 0.7GE/NR compared to the sample 0.7GO/NR. This finding can be attributed to a more significant contribution of the entanglements in the transition zone due to the stronger filler–rubber interaction in the GE/NR composite. The filler–rubber interaction in the composites was evaluated by $Q_f/Q_g$ in the Lorenz and park eq. (2). The $Q_f/Q_g$ value of 0.7GE/NR and 0.7GO/NR were 0.82 and 0.85, respectively. The lower $Q_f/Q_g$ value of 0.7GE/NR suggests a higher extent of interaction between the GE and NR matrix. Also a much higher bound rubber content (nearly twice) for GE than GO as mentioned above support this point. A fine dispersion of a small quantity of GE with higher specific surface area is enough to interact with the majority of the rubber. The GO with the hydrophilic polar oxygen functional groups does not exhibit good compatibility with the nonpolar rubber matrix.[44] Figure 8 shows the TEM images of GO/NR and GE/NR composites. It is shown that GE is well dispersed in the NR matrix [Figure 8(b)]. However, GO has an aggregation trend, which will reduce the specific surface area of GO fillers, and thus lower the interaction extent between GO and rubber matrix. Thus more entangled structures were formed, i.e., lower

**Table IV.** Network Molecular Parameters of Unfilled and Filled Rubbers

| | $G_c^{*a}$ (Mpa) | $G_e^{*b}$ (Mpa) | $d_0$ (nm) | $n_e$ | $M_c$ (g/mol) | $R_c$ (nm) |
|---|---|---|---|---|---|---|
| NR | 0.38 | 0.51 | 1.54 | 3.1 | 4822 | 7.43 |
| GO/NR | 0.37 | 0.58 | 1.46 | 2.8 | 4340 | 7.05 |
| GE/NR | 0.45 | 0.61 | 1.42 | 2.6 | 4089 | 6.84 |

$G_c^{*a}$ and $G_e^{*b}$ can be determined from the slope and y-axis interception of the linear part of the intermediate deformation in the modified Mooney plot $\sigma^*$ vs. ($\alpha$) (Figure 5), respectively.

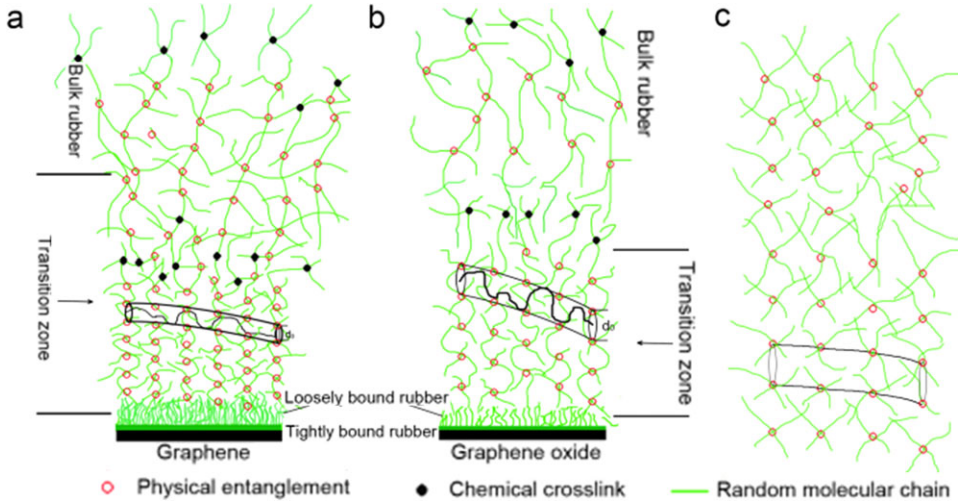


**Figure 7.** Schematic representation of the EBT model, (a) GE/NR (b) GO/NR (c) NR. [Color figure can be viewed in the online issue, which is available at wileyonlinelibrary.com.]

tube dimension in the GE/NR composites than the GO/NR. The rubber chains can also move freely during stretching as the slippage of the physical entanglements is hardly hindered in the GE/NR composites.[31] The higher slope in the Mooney–Rivlin plot of 0.7GE/NR composites (Figure 6) implies the easier slippage of the entanglement, namely, stronger ability of rubber chain movement during deformation.

The SIC of NR results from the entropy drop during elongation. The crystallization of NR chains happens in a supercooled state and the melting temperature ($T_m$) of NR increases during stretching. When $T_m$ exceeds the room temperature, the onset of the crystallization takes place eq. (16).[45]

$$\frac{1}{T_{m,s}} = \frac{1}{T_{m,0}} + \frac{\Delta S_{def}}{\Delta H} \tag{16}$$

where, $T_{m,s}$ is the melting temperature in the stretched state, $T_{m,0}$ the melting temperature in the unstretched state, $\Delta H$ the melting enthalpy, and $\Delta S_{def}$ the difference of the entropy between the stretched and unstretched states. The onset of SIC of NR composites is dependent on $\Delta S_{def}$, which is a function of strain. The simplest expression of the entropy change of deformation $\Delta S_{def}$[45] assuming the Gaussian chain is eq. (17).

$$\Delta S_{def} = -(1/2)\nu_e k_B(\alpha_0^2 + 2/\alpha_0 - 3) \tag{17}$$

where, $\nu_e$ is the experimentally determined network-chain density which calculated by using the Flory-Rehner eq. (1), $\alpha_0$ is an extension ratio at initial crystallization and it was substituted by $\alpha_r^0(b)$ (Table III). The calculated values of $\Delta S_{def}$ of the unfilled GO/NR and GE/NR are $-4.54 \times 10^3$ J/cm$^3$/K, $-3.99 \times$

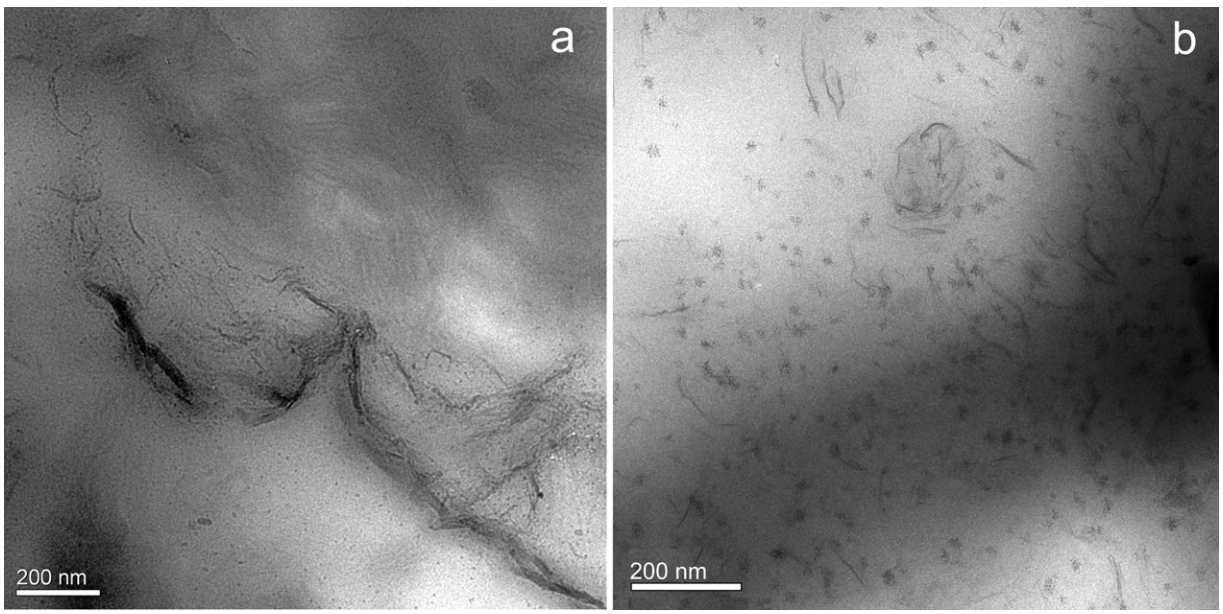


**Figure 8.** TEM images of (a) GO/NR and (b) GE/NR composites.

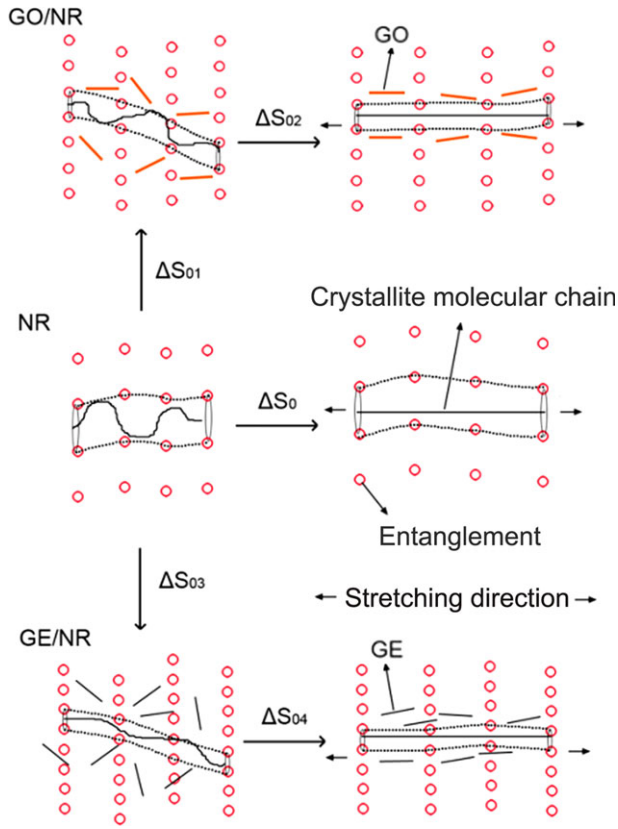


**Figure 9.** Schematic representation of structural evolution and entropy change of filled and unfilled rubber during stretching. [Color figure can be viewed in the online issue, which is available at wileyonlinelibrary.com.]

$10^3$ J/cm$^3$/K, and $-2.57 \times 10^3$ J/cm$^3$/K, respectively. Compared with the neat NR and GO/NR composites, $\Delta S_{def}$ of GE/NR composites was the lowest.

The entropy change of the filled rubber can be composed of two parts: (a) the entropy reduction caused by the addition of filler ($\Delta S_f$), which was caused by the interactions between rubber chains and the filler; (b) deformation entropy ($\Delta S_{def}$) during stretching, as shown in Figure 9. $\Delta S_f$ of GO/NR and GE/NR composites are expressed as $\Delta S_{01}$ and $\Delta S_{03}$, respectively. $\Delta S_{def}$ of GO/NR and GE/NR composites are expressed as $\Delta S_{02}$ and $\Delta S_{04}$, respectively. It is reasonable to assume that the total entropy change required for the onset of SIC in the filled and unfilled rubber is the same, i.e., $\Delta S_0 \approx \Delta S_{01} + \Delta S_{02} \approx \Delta S_{03} + \Delta S_{04}$. As $\Delta S_f$ of GE/NR composites is higher than that of GO/NR, i.e., $\Delta S_{03} > \Delta S_{01}$ due to a more ordered structure for GE/NR composites, $\Delta S_{def}$ of GE/NR composites should be lower than that of GO/NR, i.e., $\Delta S_{04} < \Delta S_{02}$, which means the onset of SIC of GE/NR composites appeared at the lowest strain.

## CONCLUSIONS

The GE/NR and GO/NR composites were prepared by an ultrasonically-assisted latex mixing process. A noticeable enhancement in tensile strength was achieved for both GO- and GE-filled NR systems, while GE has a better reinforcing effect than GO. The influences of GE and GO addition on the crystallinity of NR during stretching were determined by synchrotron WAXD. It was found that the incorporation of GE produces a faster SIC rate and a higher crystallinity compared with the GO. The same change trend in tensile strength and crystallinity suggest that SIC plays a crucial role in the NR reinforcement. The NR molecular network parameters for GE/NR and GO/NR composites were evaluated by applying the EBT model. Compared with GO, the GE have more chance to interact with rubber phase, leading to the decrease of tube dimension, and simultaneously the reduction of configurational entropy of rubber chains. GE/NR composites have a lower deformation entropy during stretching than GO/NR composites.

## ACKNOWLEDGMENTS

This work is supported by National Natural Science Foundation of China (NNSFC 51010004) and the International Science & Technology Cooperation Program of China (2010DFA54460). Professor Liangbin Li and Guoqiang Pan of National Synchrotron Radiation Laboratory (NSRL) in University of Science and Technology of China are also greatly appreciated for the help in Synchrotron WAXD experiments.

## REFERENCES

1. Gent, A. N. *Trans. Faraday Soc.* **1954**, *50*, 521.
2. Toki, S; Sics, I; Ran, S. F; Liu, L. Z.; Hsiao, B. S.; Murakami, S.; Senoo, K; Kohjiya, S. *Macromolecules* **2002**, *35*, 6578.
3. Trabelsi, S.; Albouy, P. A.; Rault, J. *Macromolecules* **2002**, *35*, 10054.
4. Toki, S; Hsiao, B. S. *Macromolecules* **2003**, *36*, 5915.
5. Joly, S.; Garnaud, G.; Ollitrault, R.; Bokobza, L. *Chem. Mater.* **2002**, *14*, 4202.
6. Carretero-Gonzalez, J.; Verdejo, R.; Toki, S.; Hsiao, B. S.; Giannelis E. P.; López-Manchado, M. A. *Macromolecules* **2008**, *41*, 2295.
7. Carretero-Gonza'lez, J.; Retsos, H.; Verdejo, R.; Toki, S.; Hsiao, B. S.; Giannelis, E. P.; Lo'pez-Manchado, M. A. *Macromolecules* **2008**, *41*, 6763.
8. Yan, N.; Xia, H. S.Wu, J. K.; Zhan, Y. H.; Fei, G. X.; Chen, C. J. *Appl. Polym. Sci.* **2013**, *127*, 933.
9. Nie, Y. J.; Huang, G. S.; Qu, L.L.; Zhang, P.; Weng, G. S.; Wu, J. R. *Polym. Adv. Technol.* **2011**, *22*, 2001.
10. Poompradub, S.; Tosaka, M.; Kohjiya, S. *J. Appl. Phys.* **2005**, *97*, 103529.
11. Weng, G. S.; Huang, G. S.; Qu, L. L.; Nie, Y. J.; Wu, J. R. *Phys. Chem. B* **2010**, *114*, 7179.
12. Lee, C.; Wei, X. D.; Kysar, J. W.; Hone, J. *Science* **2008**, *321*, 385.
13. Zhu, Y. W.; Murali, S.; Cai, W. W.; Li, X. S.; Suk, J. W.; Potts, J. R.; Ruoff, R. S. *Adv. Mater.* **2010**, *22*, 3906.
14. Zhan, Y. H.; Wu, J. K.; Xia, H. S.; Yan, N.; Fei, G. X.; Yuan, G. P. *Macromol. Mater. Eng.* **2011**, *296*, 590.

15. Zhan, Y. H.; Lavorgna, M.; Buonocore, G.; Xia, H. S. J. *Mater. Chem.* **2012**, *22*, 10464.
16. Yan, N.; Xia, H. S.; Zhan, Y. H.; Fei, G. X. *Macromol. Mater. Eng.* DOI: 10.1002/mame.201200044.
17. Yan, N.; Wu, J. K.; Zhan, Y. H.; Xia, H. S. *Plast. Rubber Comp.* **2009**, *38*, 290.
18. Wolff, S. *Rubber Chem. Technol.* **1996**, *69*, 325.
19. Ronca, G.; Allegra, G. J. *Chem. Phys.* **1975**, *63*, 4990.
20. Kästner, S. *Colloid Polym. Sci.* **1981**, *259*, 499.
21. Flory, P. J. *J. Chem. Phys.* **1977**, *66*, 5720.
22. Gottlieb, M.; Gaylord, R. *J. Polym.* **1983**, *24*, 1644.
23. Higp, P. G.; Gaylord, R. *J. Polym.* **1990**, *31*, 70.
24. Walter, B.; Ole K. *J. Chem. Phys.* **1981**, *74*, 6507.
25. Thomas, T.; Ole, K. *Macromolecules* **1991**, *24*, 5769.
26. Edwards, S. F. *Proc. Phys. Soc.* **1965**, *85*, 613.
27. Edwards, S. F. *Proc. Phys. Soc.* **1967**, *92*, 9.
28. Leblanc, J. L. *Plast. Rubber Proc. Technol.* **1994**, *10*, 110.
29. Funt, J. M. *Rubber Chem. Technol.* **1988**, *61*, 842.
30. Heinrich, G.; Vilgis, T. A. *Macromolecules* **1993**, *26*, 1109.
31. López-Manchado, M. A.; Valentín, J. L.; Carretero, J.; Barroso, F.; Arroyo, M. *Eur. Polym. J.* **2007**, *43*, 4143.
32. Hummers, W. S.; Offeman, R. E. *J. Am. Chem. Soc.* **1958**, *80*, 1339.
33. Flory, P. J. Principles of Polymer Chemistry; Cornell University Press: New York, **1953**; p 576.
34. Lorenz, O.; Parks, C. R. *J. Polym. Sci.* **1961**, *50*, 299.
35. Leblanc, J. L.; Hardy, P. *Kautsch Gummi Kunstst* **1991**, *44*, 1119.
36. Flory, P. J. *Ind. Eng. Chem.* **1946**, *38*, 417.
37. Wang, M. C.; Guth, E. J. *Chem. Phys.* **1952**, *20*, 1144.
38. Marquardt, D. W. *J. Soc. Ind. Appl. Math.* **1963**, *11*, 434.
39. Rault, J.; Marchal, J.; Judeinstein, P.; Albouy, P. A. *Macromolecules* **2006**, *39*, 8356.
40. Tosaka, M.; Murakami, S.; Poompradub, S.; Kohjiya, S. *Macromolecules* **2004**, *37*, 3299-3309.
41. Klug, H. P.; Alexander, L. E. In X-ray Diffraction Procedures for Polycrystalline and Amorphous Materials, 2nd ed.; Wiley Interscience: New York, **1974**, p 687.
42. Klüppel, M.; Schramm, J. *Macromol. Theory Simul.* **2000**, *9*, 742.
43. Schikoweky, M. Diploma Thesis. Technical University Merseburg (German), **1984**.
44. Paredes, J. I.; Villar-Rodil, S.; Martinez-Alonso, A.; Tascon, J. M. D. *Langmuir* **2008**, *24*, 10560.
45. Tosaka, M. *Macromolecules* **2009**, *42*, 6166.